

One-Dimensional Sliding of p53 Along DNA Is Accelerated in the Presence of Ca^{2+} or Mg^{2+} at Millimolar Concentrations

Agato Murata [1,2], Yuji Ito [1,2], Risa Kashima [3,5], Saori Kanbayashi [1], Kei Nanatani [4,6], Chihiro Igarashi [1,2], Masaki Okumura [1], Kenji Inaba [1], Takashi Tokino [3], Satoshi Takahashi [1] and Kiyoto Kamagata [1]

*1 - **Institute for Multidisciplinary Research for Advanced Materials,** Tohoku University, Katahira 2-1-1, Aoba-ku, Sendai 980-8577, Japan*
*2 - **Department of Chemistry,** Graduate School of Science, Tohoku University, Sendai 980-8578, Japan*
*3 - **Department of Medical Genome Sciences,** Research Institute for Frontier Medicine, Sapporo Medical University, Chuo-ku, Sapporo 060-8556, Japan*
*4 - **Department of Biomolecular Engineering,** Graduate School of Engineering, Tohoku University, Sendai 980-8579, Japan*

***Correspondence to Satoshi Takahashi and Kiyoto Kamagata:** st@tagen.tohoku.ac.jp; kamagata@tagen.tohoku.ac.jp*
http://dx.doi.org/10.1016/j.jmb.2015.06.016
Edited by S. Kowalczykowski

Abstract

One-dimensional (1D) sliding of the tumor suppressor p53 along DNA is an essential dynamics required for its efficient search for the binding sites in the genome. To address how the search process of p53 is affected by the changes in the concentration of Mg^{2+} and Ca^{2+} after the cell damages, we investigated its sliding dynamics at different concentrations of the divalent cations. The 1D sliding trajectories of p53 along the stretched DNA were measured by using single-molecule fluorescence microscopy. The averaged diffusion coefficient calculated from the mean square displacement of p53 on DNA increased significantly at the higher concentration of Mg^{2+} or Ca^{2+}, indicating that the divalent cations accelerate the sliding likely by weakening the DNA–p53 interaction. In addition, two distributions were identified in the displacement of the observed trajectories of p53, demonstrating the presence of the fast and slow sliding modes having large and small diffusion coefficients, respectively. A coreless mutant of p53, in which the core domain was deleted, showed only a single mode whose diffusion coefficient is about twice that of the fast mode for the full-length p53. Thus, the two modes are likely the result of the tight and loose interactions between the core domain of p53 and DNA. These results demonstrated clearly that the 1D sliding dynamics of p53 is strongly dependent on the concentration of Mg^{2+} and Ca^{2+}, which maintains the search distance of p53 along DNA in cells that lost homeostatic control of the divalent cations.

© 2015 Elsevier Ltd. All rights reserved.

Introduction

The tumor suppressor p53 is the transcription factor that controls the cellular fate as a guardian of the genome [1,2]. p53 induces cell cycle arrest, apoptosis, or DNA repair upon different types of cellular stresses. p53 has four domains: N-terminal domain, core domain, tetramerization domain, and C-terminal domain. A flexible linker connects the core domain and the tetramerization domain. The core and tetramerization domains have specific folded structures, while the other domains are disordered. The core and C-terminal domains are respectively related to the binding of p53 to DNA in sequence-specific and nonspecific manners. The specific binding of p53 to the target DNA sequence causes the transactivation of gene products leading to the various cell fates. In 50% of human cancers, the mutations of p53 gene are found, which are located in the core domain and prevent the specific binding to DNA [3]. Due to its importance, the mechanism by which p53 searches for its binding sites among huge DNA has been the focus of intensive investigations [4–8].

The one-dimensional (1D) sliding of p53 along DNA is one of the essential dynamics in the search

process and has been directly investigated by single-molecule techniques. The sliding of p53 along the fixed DNA was first observed using a high-speed atomic force microscopy [4]. Subsequently, the sliding of p53 was observed using fluorescence microscopy by tracking the position of fluorescent-labeled p53 bound to DNA stretched by a flow [5,6]. The diffusion coefficient for the sliding dynamics of p53 was determined and was 0.16 $\mu m^2/s$ [5]. The C-terminal domain promotes the diffusion along the DNA, while the core domain suppresses the diffusion [5]. The diffusion coefficient does not depend on the concentration of a monovalent cation, K^+ [5,6]. The DNA sequence slightly affects the diffusion [7]. It is proposed that p53 diffuses along DNA and searches for the target sites by repeating the transient association of the core domains to DNA and their dissociation, which was supported by the course-grained molecular dynamics simulations [8]. These results demonstrate the importance of the sliding dynamics of p53 along DNA.

The sliding dynamics of p53 might be regulated by the cellular conditions under various cell phases. For example, the cell death is deeply linked to Ca^{2+} signaling [9,10]. Under some stress, the expression level of p53 is elevated and the Ca^{2+} concentration is increased [11,12]. The elevated concentration of Ca^{2+} in nucleus induces chromatin unfolding and promotes the gene transcriptions regulated by Ca^{2+}-binding proteins, as well as the digestion of nuclear DNA by Ca^{2+}- and Mg^{2+}-dependent endonucleases. In addition, Mg^{2+} deficiency induces the elevated expression of p53, resulting in cell cycle arrest [13]. Since these divalent cations bind tightly and specifically to DNA [14–19], the sliding dynamics of p53, dictated by the interaction between p53 and DNA, would also be modulated by the divalent cations. In fact, early investigations of the lac repressor suggested that Mg^{2+} alters the 1D sliding along DNA and the binding ability to DNA [20,21]. Accordingly, we hypothesize that the loss of homeostatic control for divalent cations such as Ca^{2+} and Mg^{2+} might regulate the target search of p53.

In this study, we investigated the effect of the divalent cations on the sliding dynamics of p53 along DNA. To this end, we prepared a stable tetrameric mutant of p53 [the pseudo-WT (*w*ild *t*ype)] that can maintain the specific binding ability to DNA sufficient for the single-molecule fluorescence measurements. Using the pseudo-WT, we examined the nonspecific binding ability relevant to the sliding dynamics. We found that the dissociation rate constant was increased as the increase in the concentration of Mg^{2+} or Ca^{2+}. We observed the sliding of p53 along DNA at the single-molecule level at different concentrations of Mg^{2+} and Ca^{2+} and found that the sliding of p53 was significantly accelerated by adding the millimolar concentration of the divalent cations. The analysis of the sliding trajectories further suggests that p53 possesses two sliding modes with different diffusion coefficients. We also prepared a coreless mutant of p53, in which the core domain and the N-terminal domain were deleted, and found that a single diffusion mode was observed in the coreless mutant. We propose that the increased diffusion of p53 in the presence of the divalent cations occurs as the result of a weakening of the DNA–p53 interaction upon the binding of the divalent cations to DNA.

Results

Construction of the stabilized mutant of p53 with a single exposed cysteine

In our early trials, we prepared the human WT p53 by expressing the protein with GST (*g*lutathione *S*-*t*ransferase) tag in *Escherichia coli*, followed by the cleavage of the tag and the purification. The oligomeric state of the purified protein was examined by gel filtration, SDS-PAGE for the cross-linked p53 and native PAGE. In addition, the DNA binding activity was examined by electrophoretic mobility shift assay. We succeeded in the preparation of the tetrameric p53 having the specific binding ability toward the target DNA; however, it was difficult to reproduce the activity especially after frozen storages. This is likely due to the aggregation-prone property and/or the incomplete folding of the core domain of the WT p53 [22]. In addition, the labeling of the WT p53 by fluorophore for the single-molecule measurements likely affected its activity because some of the four solvent-exposed cysteines are located in the binding site for DNA (Supplementary Fig. 1 and the supplementary text). We concluded that the WT p53 is not suitable for the investigation based on the single-molecule fluorescence measurements. The instability of the WT p53 was similarly reported in previous investigations [5,22,23].

To obtain reproducible results, we prepared a thermostable mutant having a single solvent-exposed cysteine for the labeling. The mutations introduced are C135V, C141V, W146Y, C182S, V203A, R209P, C229Y, H233Y, Y234F, N235K, Y236F, T253V, and N268D, which are based on thermostable mutations reported as ST7 [23]. C176, C238, and C242 are left intact due to their involvement in coordination to Zn^{2+}, which is required for the binding of p53 to DNA. C124A, C275A, and C277A are introduced to remove the rest of the cysteines, and K292C is introduced as the single labeling site. We name the thermostable mutant pseudo-WT. The pseudo-WT p53 with GST tag expressed in *E. coli* was purified after cleavage of the tag. The yield of the purified mutant was 1.7 mg per 1 L of culture, which was improved significantly compared with the yield, 0.4 mg per 1 L of culture, of the WT p53. The increased yield is likely the result of

the codon optimization for *E. coli* and the increased stability of the mutant. Based on the SDS-PAGE analysis for the sample cross-linked by glutaraldehyde, we confirmed that the pseudo-WT formed a tetramer (Supplementary Fig. 2a). In addition, the molecular weight of the pseudo-WT estimated by the native PAGE assay was consistent with that of the tetramer obtained in gel filtration [24] (Supplementary Fig. 2b). The pseudo-WT p53 was labeled with a fluorescence dye, ATTO532, at the labeling efficiency of 1.4 dyes per monomer.

To further examine the binding activity of the pseudo-WT p53, we performed two types of examinations. First, we performed electrophoretic mobility shift assay (Supplementary Fig. 2c and the supplementary text). The purified p53 was strongly bound to the specific target sequence with 30 bp (spDNA). In contrast, in the presence of a competitor that is 100 bp of the double-stranded DNA without the target site, the amount of the p53–spDNA complex was suppressed. Furthermore, in the presence of an antibody PAb421, which binds to the C-terminal domain of p53 and enhances the binding of p53 to spDNA, the p53–spDNA–PAb421 complex was observed even in the presence of the competitor. These results are consistent with those of a previous report [25]. Second, we performed the titration of the fluorescence anisotropy of FAM attached to spDNA and 30 bp of a nonspecific sequence of double-stranded DNA (nspDNA) at different concentrations of the p53 mutant [23,26]. The anisotropies of spDNA and nspDNA labeled by FAM showed the saturation behavior at the increased concentration of the p53 mutant, suggesting the 1:1 binding (Fig. 1a). The anisotropy data were well fitted by a two-state model, in which one tetramer of p53 binds to one DNA with an apparent dissociation constant [see Eqs. (3) and (4) in Materials and Methods]. To prevent the dissociation of the tetramer, we performed all the measurements in this study within 50 min after the dilution of the stock solution [27]. The apparent dissociation constants for the binding of p53 to spDNA and nspDNA were 0.8 ± 0.1 and 8 ± 1 nM per tetramer, respectively. Taking the difference under the experimental conditions such as salt concentration into account, we conclude that the apparent dissociation constant for spDNA is consistent with the reported values, which were on the order of nanomolars [23,26]. The observation that the apparent dissociation constant for spDNA is lower compared to that for nspDNA indicates that the pseudo-WT p53 retained the ability to bind the target DNA sequence specifically.

We confirmed that the oligomeric state and the activity of the pseudo-WT p53 were not altered even after the frozen storages (data not shown). Thus, these results demonstrated that the constructed p53 is stable and possesses the specific DNA binding ability and is suitable for the further investigations based on fluorescence microscopy.

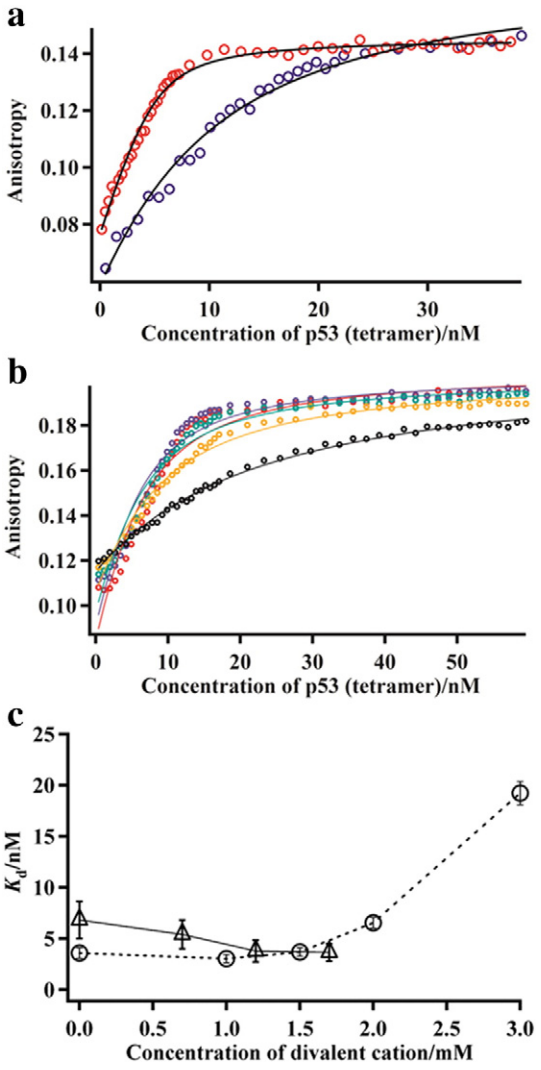


Fig. 1. (a) Static fluorescence-anisotropy measurements for the titration of the pseudo-WT p53 against spDNA (red circle) and nspDNA (blue circle) labeled by FAM in the presence of 2 mM Mg^{2+}. The curves were the best-fitted curves obtained by using Eqs. (3) and (4). (b) Static fluorescence-anisotropy measurements for the titration of the pseudo-WT p53 against nspDNA in the presence of 0–3 mM Mg^{2+}. Red, blue, green, orange, and black circles were the data in the presence of 0, 1, 1.5, 2, and 3 mM Mg^{2+}, respectively. The curves were the best-fitted curves. (c) The apparent dissociation constant of the pseudo-WT p53 from nspDNA at the different concentrations of the divalent cations. Triangles and circles represent data obtained in the presence of Ca^{2+} and Mg^{2+}, respectively. The error bars represent the fitting error.

Effect of the divalent cations on the nonspecific binding of p53 to DNA

To understand possible roles of the divalent cations on the 1D sliding dynamics of p53 along nonspecific DNA, we first examined the effect of the divalent cations on the equilibrium dissociation constant of p53

from nspDNA at the ensemble level. We performed the titration of the fluorescence anisotropy of FAM attached to nspDNA at different concentrations of the pseudo-WT p53 under various Mg^{2+} concentrations (Fig. 1b). The apparent dissociation constant obtained by fitting the anisotropy data was constant at the Mg^{2+} concentration below 1.5 mM, but it increased above 2 mM (Fig. 1c), confirming that Mg^{2+} at the millimolar concentration affects the p53–DNA interaction. We also examined the effect of Ca^{2+} on the apparent dissociation constant, which was slightly decreased as the increase in [Ca^{2+}], suggesting the effect of Ca^{2+} is different from that of Mg^{2+} (Fig. 1c and Supplementary Fig. 3).

To further examine the effect of the divalent cations on the p53–DNA interaction, we constructed a stopped-flow, fluorescence-anisotropy apparatus and measured the dissociation kinetics of the pseudo-WT p53 from nspDNA. The fluorescence anisotropy of the labeled nspDNA bound to p53 decreased after a mixing with an excess amount of spDNA with no fluorescent dye, corresponding to the dissociation of p53 from nspDNA (Fig. 2a). We fitted the obtained time courses with a single exponential, and we obtained the apparent rate constant for the dissociation of p53 from nspDNA, k_{off}. The obtained k_{off} value in the absence of Mg^{2+} is consistent with the reported residence time, less than 1 s, of p53 on DNA [23]. As shown in Fig. 2b, the k_{off} value increased significantly with the concentration of Mg^{2+}. We further examined the effect of Ca^{2+} on the dissociation kinetics and observed that the k_{off} value increased similarly with the concentration of Ca^{2+} (Fig. 2b and Supplementary Fig. 4). Thus, these results clearly demonstrated that the divalent cations can accelerate the dissociation kinetics of p53 from DNA without the target sequence.

We found that the divalent cations affect the nonspecific binding of p53. We propose that Mg^{2+} and Ca^{2+} may weaken the direct interaction between p53 and DNA, resulting in the acceleration in the dissociation of p53 from DNA. Considering the dependence of k_{off} on the concentration of divalent cations, we expect that the 1D sliding of p53 along DNA might be altered upon the increase in the concentration of the divalent cations.

Single-molecule observation of the 1D sliding of p53 and the determination of the diffusion coefficient

To observe the sliding of p53, we prepared the stretched DNA in the flow cell under flow pressure as follows. The flow cell consists of a coverslip, a glass slide, and a spacer [28]. The width and height of the

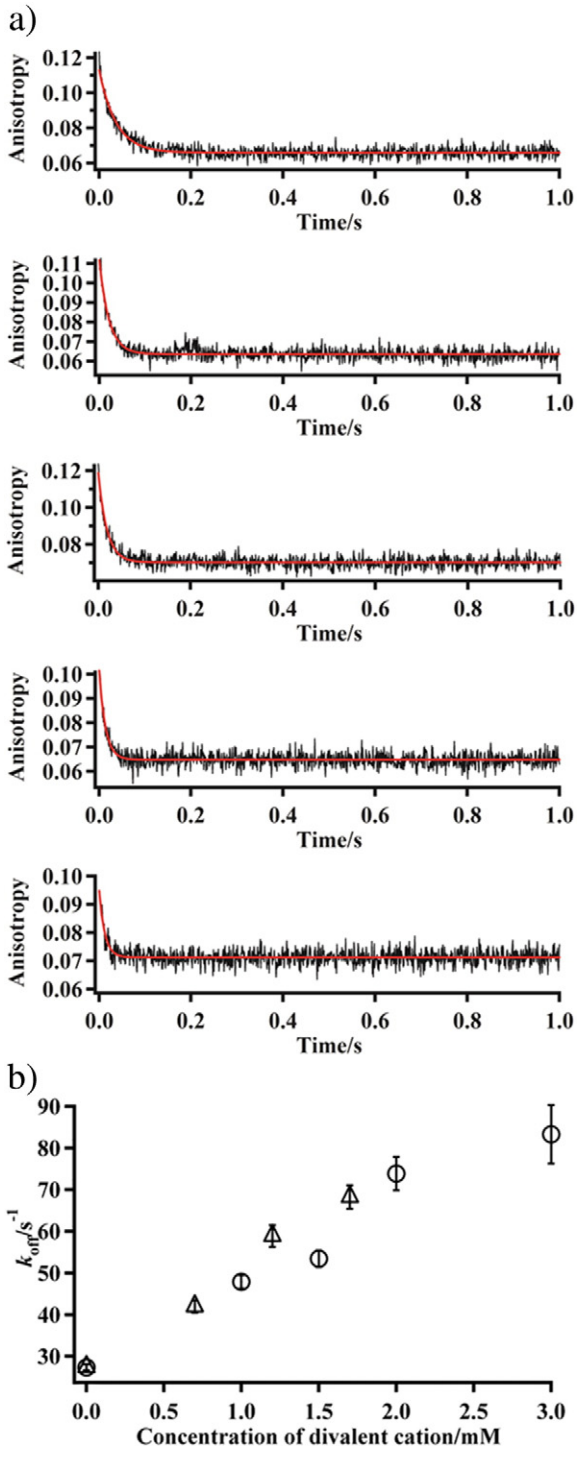


Fig. 2. (a) Kinetic fluorescence-anisotropy measurements for the dissociation process of the pseudo-WT p53 from nspDNA labeled by FAM. Black traces from top to bottom were the data in the presence of 0, 1, 1.5, 2, and 3 mM Mg^{2+}, respectively. Red curves were the best-fitted curves with a single exponential. (b) The apparent dissociation rate constant of the pseudo-WT p53 from nspDNA at the different concentrations of divalent cations. Triangles and circles represent data obtained in the presence of Ca^{2+} and Mg^{2+}, respectively. The error bars represent the fitting error.

flow path in the flow cell were 3–4 mm and 0.1 mm, respectively. The inner surface of the coverslip was coated by polyethylene glycol (PEG) conjugated with biotin (Fig. 3a). The DNA with both biotinylated ends [29,30] was then introduced to the cell in the presence of neutravidin and was attached on the coverslip at one end. λDNA, which does not contain the target sites for p53, was used to investigate the sliding along nonspecific DNA. The flow was applied to stretch the DNA at the volume flow rate of 500 μL/min. The averaged line speed of the solution in the flow cell was estimated to be ~24 mm/s. The flow rate at the DNA estimated from the mean distance (0.2 μm) between the DNA and the coverslip surface was ~280 μm/s [6]. The mean extension of the DNA was estimated to be 80% from Weissenberg number (290) that represents

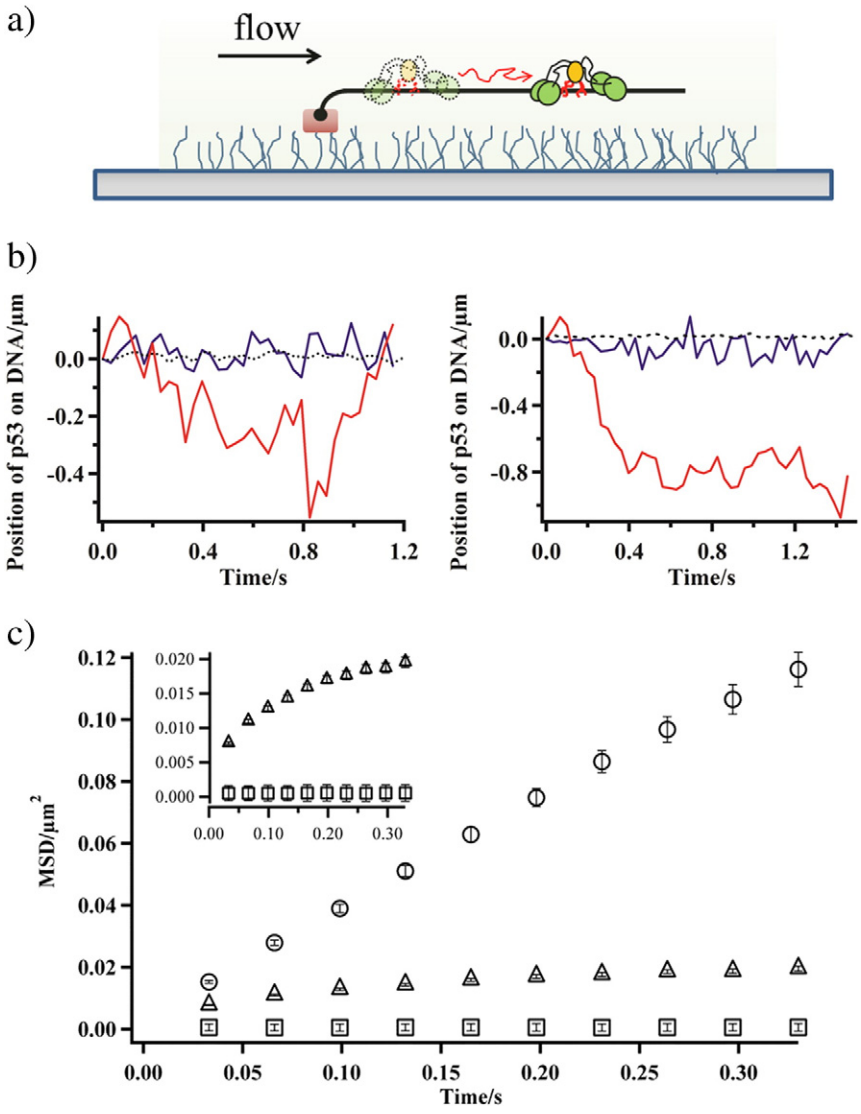


Fig. 3. (a) Schematic representation of the setup for the single-molecule experiments. One end of λDNA (black line) was labeled with biotin and attached on the coverslip of the flow cell via neutravidin (brown). The coverslip was coated with PEG conjugated with biotin (blue). The TIRF illumination based on an oil immersion objective was used to observe the position of p53 labeled by ATTO532 along the DNA stretched by flow. (b) Typical trajectories for the movement of the pseudo-WT p53 bound on DNA along the longitudinal (red) and transverse (blue) directions in the presence of 2 mM Mg^{2+}. The flow pressure was applied from a positive to a negative value of the longitudinal direction. Dotted lines represent trajectories along the longitudinal direction of the p53 mutant adsorbed on the surface of the flow cell. (c) Time courses of the averaged MSD of the pseudo-WT p53 in the longitudinal (circles) and transverse (triangles) axes in the presence of 2 mM Mg^{2+}. Squares are the averaged MSD for the molecules adsorbed on the surface of the flow cell. The inset shows the same data in the expanded scale. The errors of the average are the standard error.

the dimensionless flow strength [31]. We observed that 5–20 DNAs were lined up along the flow direction in the field of view with a diameter of 30 μm in total internal reflection fluorescence (TIRF) microscopy.

The TIRF microscopy was constructed to visualize the 1D sliding of p53 along the stretched DNA. The excitation light from the 532-nm laser was reflected by a dichroic mirror and was introduced to a peripheral portion of an objective corresponding to *N.A.* at around 1.40. The optical configuration enabled the sample illumination with the total internal reflection mode. The fluorescence was collected by the same objective and was detected by TDI-EM CCD camera after passing through the dichroic mirror. The labeled p53 was introduced into the flow cell in the presence of 2 mM Mg^{2+} and was imaged as fluorescent spots. Two-dimensional images were taken at a 33-ms interval.

To examine the spatial resolution of the current system, we first selected the spots adsorbed on the cell surface and analyzed their behaviors. Figure 3b shows typical trajectories of the pseudo-WT p53 obtained by tracking the center of the fluorescent spots in the two-dimensional images observed at each time. While some of the spots showed the movement along the longitudinal (red) and transverse (blue) directions, the rest of the spots did not move (dotted), suggesting that the latter spots correspond to the adsorbed p53 on the surface. The spots that did not move in the longitudinal direction did not move in the transverse direction either (data not shown), further confirming that the spots correspond to p53 directly attached to the cell surface. By tracking the center of the adsorbed spots and calculating the standard deviation of the center, we estimated the accuracy of the localization of the molecule in the current experiments to be 0.02 μm on average ($N \sim 103$).

We performed the following data analysis to select p53 attached on DNA and sliding along it and to exclude p53 adsorbed on the cell surface. First, we obtained time series of x and y coordinates of all the fluorescence spots in the images, which respectively correspond to the longitudinal and traverse axes of DNA, and we selected data having more than 15 data points. Second, we segmented the time series of the y coordinate into every 10 data points and calculated the mean square displacements (MSDs) at a 165-ms interval for each segment. We term the values as local MSD. Third, we selected the trajectories in which all the values of the local MSDs were larger than 0.0015 μm^2. This criterion could remove the molecules adsorbed on the coverslip. We obtained 182 trajectories whose averaged time duration was 0.8 s in the presence of 2 mM Mg^{2+}. The red and blue traces shown in Fig. 2b correspond to the trajectories along the longitudinal and transverse directions, respectively, selected by the abovementioned criteria. These trajectories show much larger movements than those of the molecules adsorbed on the coverslip, further confirming the removal of the adsorbed molecules in the selected molecules. It is apparent that the longitudinal movement, which corresponds to the sliding along DNA, is much larger than the transverse movement.

The trajectories of p53 thus selected should reflect the fluctuation due to the sliding of p53 along DNA and the fluctuation of the singly fixed DNA in the flow. To examine the sliding property of p53, we plotted the time dependence of MSD averaged over all the selected trajectories (Fig. 3c). The averaged MSD in the longitudinal axis shows a linear relationship against the time interval, confirming that the sliding of p53 is Brownian in nature. The averaged diffusion coefficient D, obtained by fitting the slope of the MSD plots with $2D$, was 0.181 ± 0.006 $\mu m^2/s$ and is consistent with the value in the previous report (0.16 $\mu m^2/s$) [5]. As we will explain below, a portion of the molecules was affected by the flow and showed a drift; however, the drift was not significant and the MSD showed mostly linear dependency on the short time intervals. In contrast, the transverse movement was highly restricted, which can be attributed to the fluctuation of the DNA [5]. The averaged MSD in the transverse axis was saturated within ~0.2 s, which corresponds to the relaxation time of the fluctuation of the DNA. In large part of the stretched DNA except for the free edge, the fluctuation in the longitudinal axis was reported to be less than or comparable to that in the transverse axis [5]. Thus, we conclude that the fluctuation of the DNA should not significantly contribute to the observed fluctuation of p53 along the longitudinal axis.

Overall, we established a method to characterize the sliding dynamics of p53 by using TIRF microscopy. In addition, the detailed analysis of the observed data characterized that the sliding of p53 occurred as a diffusive motion.

The increased concentration of divalent cations accelerates the 1D sliding of p53

To examine the effect of the divalent cations in the 1D sliding of p53, we performed the single-molecule measurements at various Mg^{2+} concentrations. Figure 3b and Supplementary Fig. 5 show typical trajectories of the pseudo-WT p53 attached on the DNA in the presence of 0–3 mM Mg^{2+}. The sliding in the longitudinal axis was enhanced, as the concentration of Mg^{2+} was increased to more than 2 mM. The averaged MSDs show a linear relationship against time, suggesting that the simple diffusion governs the sliding of p53 at different concentrations of Mg^{2+} (Fig. 4a). As shown in Fig. 4c, the averaged diffusion coefficient increased as the increase in the concentration of Mg^{2+}. The averaged diffusion coefficient in the presence of 2 mM Mg^{2+} was five

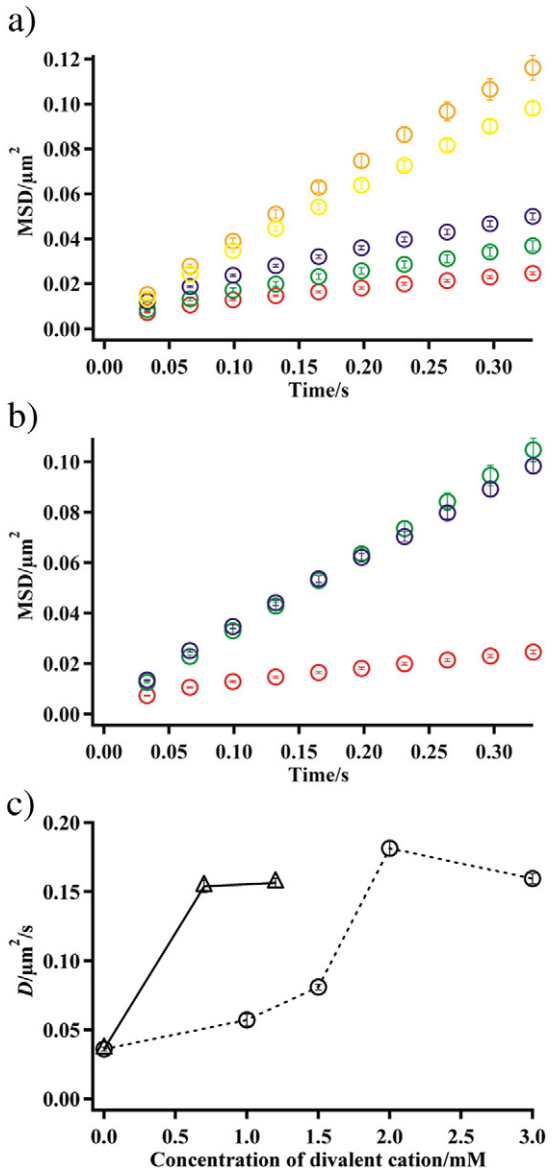


Fig. 4. (a) Time courses of the averaged MSD of the pseudo-WT p53 observed in the presence of 0–3 mM Mg^{2+}. The red, green, blue, orange, and yellow circles are the averaged MSD values in the presence of 0, 1, 1.5, 2, and 3 mM Mg^{2+}, respectively. (b) Time courses of the averaged MSD of the pseudo-WT p53 observed in the presence of 0–1.2 mM Ca^{2+}. The red, green, and blue circles are the averaged MSD values in the presence of 0, 0.7, and 1.2 mM Ca^{2+}, respectively. (c) The averaged diffusion coefficients of the pseudo-WT p53 at the different concentrations of divalent cations. Triangles and circles represent data obtained in the presence of Ca^{2+} and Mg^{2+}, respectively. The errors of the average are the standard error.

times larger than that in the absence of Mg^{2+}. Thus, these results demonstrate that Mg^{2+} dramatically alters the sliding property of p53.

We next investigated whether or not the other divalent ion, Ca^{2+}, affects the 1D sliding of the pseudo-WT p53. Figure 4b and c shows the Ca^{2+} dependence of the averaged MSD curve and the averaged diffusion coefficient, respectively. Similar to the observations for Mg^{2+}, the averaged diffusion coefficient increased in the presence of 0.7–1.2 mM Ca^{2+}. The increase of the diffusion coefficient occurred at the lower concentration of Ca^{2+} compared to that of Mg^{2+}. Thus, the changes in the concentrations of Ca^{2+} also alter the 1D sliding dynamics of p53 along DNA.

The loss of the homeostatic controls of the divalent cations in cells was observed in the early stage of apoptosis and cell cycle arrest [11–13]. In such situations, p53 searches for and binds to the target site resulting in apoptosis or cell cycle arrest. In this study, we found that the changes in the concentrations of the divalent cations in the range experienced in the cells that lost homeostatic controls drastically alter the 1D sliding dynamics of p53. In contrast, the monovalent cation does not affect the diffusional motion in the sliding of p53 [5]. These results suggest that the changes in the concentrations of divalent cations might also regulate the search process of p53 for the binding site.

Heterogeneity of the sliding of p53

To further examine the mechanism by which the 1D sliding is controlled by divalent cations, we next plotted the distributions of displacements for the observed trajectories at the time interval of 165 ms and at different concentrations of Mg^{2+} (Fig. 5). If p53 shows a simple diffusion, a single Gaussian distribution should be observed in the histogram. If p53 shows drifts caused by the flow pressure, the shift of the peak center in the displacement distribution should be observed. Indeed, the observed distributions clearly deviated from the single Gaussian and are likely the sum of two Gaussians. One of the possible reasons for this may be the heterogeneity for the sliding of p53. The deviation from the single Gaussian becomes more apparent at the longer time interval (Supplementary Fig. 6). We could fit all the distributions by the sum of two Gaussians, each having different diffusion coefficients and drift velocities as expressed in Eq. (1):

$$P(\delta x) = \sum_{i=1}^{2} \frac{A_i}{\sqrt{4\pi D_i \delta t}} \exp\left(-\frac{(\delta x + v_i \delta t)^2}{4 D_i \delta t}\right), \quad (1)$$

where δx, A_i, v_i, and D_i are the displacement in the time interval, the amplitude, the drift velocity, and the apparent diffusion coefficient of the ith component, respectively. The result of the fitting was shown in Fig. 5 and clearly demonstrates that the sliding dynamics of the pseudo-WT p53 is heterogeneous and can be described by two components. We refer

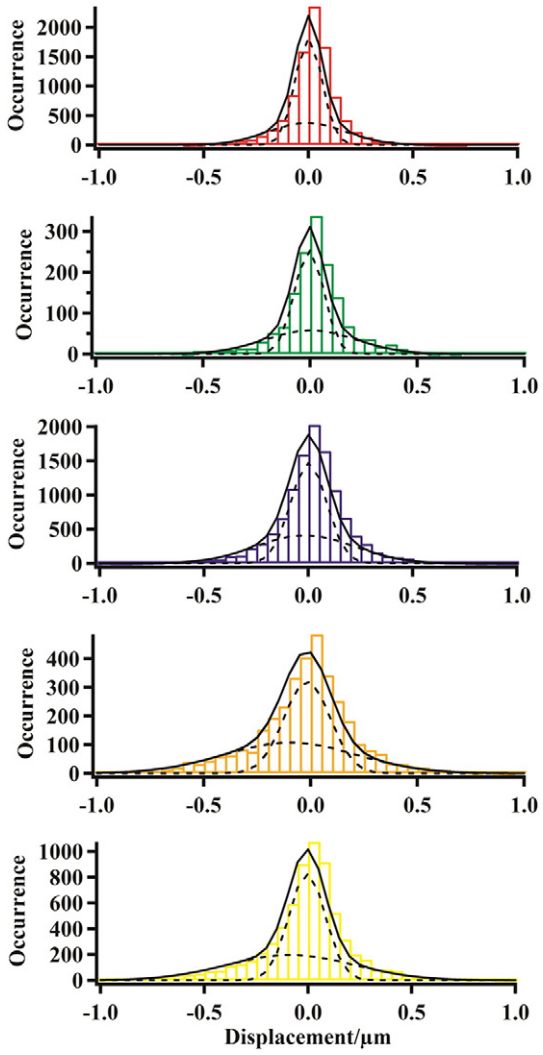


Fig. 5. The Mg^{2+} concentration dependence of the displacement distributions at the time interval of 165 ms. Red, green, blue, orange, and yellow distributions are calculated from the data of the pseudo-WT p53 in the presence of 0, 1, 1.5, 2, and 3 mM Mg^{2+}, respectively. Black curves represent the best-fitted curves obtained by using Eq. (1). Broken curves are the distributions of each mode.

to these two components as the fast and slow modes depending on the diffusion coefficients.

Figure 6 shows the Mg^{2+} concentration dependence of the apparent diffusion coefficient and the drift velocity for the fast and slow modes estimated from the fitting of the data in Fig. 5. The apparent diffusion coefficients estimated for the slow mode did not significantly depend on the Mg^{2+} concentration. In fact, the distribution width for the slow mode did not apparently depend on the time interval (Supplementary Fig. 6), suggesting that the observed distribution for the slow mode might be ascribed to the fluctuation of the DNA and that p53 in the slow

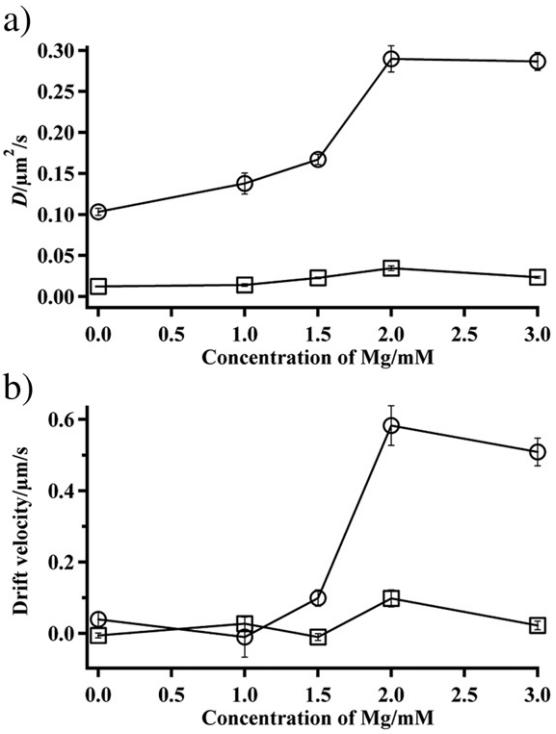


Fig. 6. The Mg^{2+} concentration dependence of the apparent diffusion coefficients (a) and the drift velocities (b) for the fast (circles) and slow (squares) modes of the pseudo-WT p53 obtained by the fitting of the displacement distributions at the time interval of 165 ms shown in Fig. 5. The error bars are the fitting errors.

mode might be stacked on the DNA. The fluctuation along the traverse direction in the slow mode was larger than that of the adsorbed molecules, suggesting that a transient interaction of p53 to the cell surface is not the origin of the slow mode. In accordance with the interpretation, the drift velocity of the slow mode was almost 0. In contrast, as the concentration of Mg^{2+} increased, the apparent diffusion coefficient and the drift velocity of the fast mode were accelerated significantly. The fractions of the fast and slow modes were respectively 49 ± 3% and 51 ± 3% at 2 mM Mg^{2+} and did not significantly depend on the concentration of Mg^{2+} (Supplementary Fig. 7). We could not detect clear transitions between the fast and slow modes in the trajectories within 330 ms, suggesting that the transition will occur at the longer time interval. Supplementary Figure 8 demonstrated that the two modes were also present when Ca^{2+} was added. The diffusion coefficients and the fractions of the two modes observed at 0.7–1.2 mM Ca^{2+} were similar to those at 2–3 mM Mg^{2+}. Thus, the detailed analysis of the displacement distribution suggests that the two modes are present in the sliding dynamics of p53 along DNA and that the fast mode shows the accelerated diffusion in the presence of Mg^{2+} and Ca^{2+}.

We conducted various control experiments to rule out the possibility that the observed two modes are caused by some artifacts. The observed two modes are not the result of the heterogeneity in the sample identity, in the oligomeric state, in the affinity to DNA, or in the sample labeling (Fig. 1; Supplementary Figs. 2, 4, 9, and 10; and the supplementary text). We can also rule out the transient adsorption of p53 to the cell surface as the possible origin of the slow mode (see the supplementary text). These control experiments strongly suggest that the presence of the two modes should be ascribed to the inherent heterogeneity in the interaction between p53 and DNA.

The core domain of p53 causes the heterogeneity of the sliding

The core domain, which is responsible for the specific binding of p53 to the target sequence of DNA, also suppresses the 1D sliding [5], suggesting that the core domain interacts with DNA in the sliding process. It can be further assumed that heterogeneous interactions between the core domain and DNA might cause the two sliding modes. To examine the roles of the core domain in the heterogeneous sliding dynamics of p53, we constructed a coreless variant of p53 in which the core and N-terminal domains were deleted from the pseudo-WT p53, and we labeled the variant with ATTO532 (see the supplementary text). The sliding dynamics of the coreless mutant in the presence of 2 mM Mg^{2+} was examined in the flow cell coated by 2-methacryloyloxyethyl phosphorylcholine (MPC) polymer (see the supplementary text). We analyzed 94 single-molecule trajectories of the coreless mutant and plotted their distribution of displacement at the time interval of 165 ms (Fig. 7a).

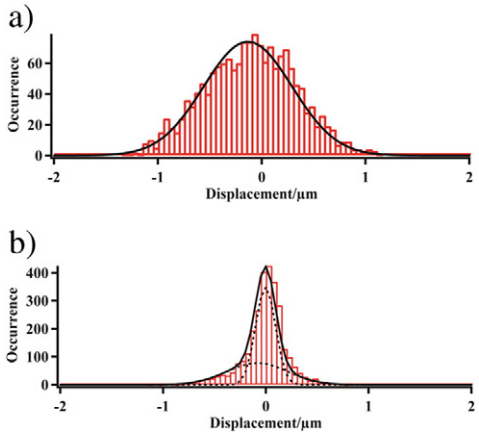


Fig. 7. Comparison of the displacement distributions observed for the coreless mutant (a) and the pseudo-WT (b) of p53 at the time interval of 165 ms in the presence of 2 mM Mg^{2+}. Black curves represent the best-fitted curves obtained by using Eq. (2) for (a) or Eq. (1) for (b). Broken curves in (b) are the distributions of each mode.

In contrast to the heterogeneous distribution observed for the pseudo-WT, the distribution for the coreless mutant becomes homogeneous and can be well fitted by a single Gaussian expressed in Eq. (2):

$$P(\delta x) = \frac{A}{\sqrt{4\pi D\delta t}} \exp\left(-\frac{(\delta x + v\delta t)^2}{4D\delta t}\right). \quad (2)$$

The diffusion coefficient, D, estimated by the fitting was 0.54 ± 0.02 μm^2/s, and the drift velocity, v, was 0.81 ± 0.07 μm/s. The estimated diffusion coefficient was close to that obtained in Ref. [5] (0.776 ± 0.098 μm^2/s). We repeated the same measurements of the pseudo-WT p53 under the identical experimental condition (Fig. 7b) and reproduced the two distributions. The diffusion coefficients of the fast and slow modes for the pseudo-WT p53 were 0.26 ± 0.02 and 0.03 ± 0.02 μm^2/s, respectively. The drift velocities of the fast and slow modes were 0.51 ± 0.06 and 0.02 ± 0.02 μm/s, respectively. These values of the pseudo-WT p53 in the cell coated by MPC polymer coating were identical with those in the cell coated by PEG coating (Fig. 6). These results demonstrate clearly that the core domain causes the heterogeneity in the 1D sliding dynamics of p53.

The diffusion coefficient of the coreless mutant, 0.54 ± 0.02 μm^2/s, which is ca two times larger than that of the fast mode of the pseudo-WT obtained under the identical condition (0.26 ± 0.02 μm^2/s). It suggests that the core domain interacts weakly with DNA in the fast mode. In contrast, the diffusion coefficient of the coreless mutant was 19 times larger than that of the slow mode, suggesting that the core domain interacts strongly with DNA and retards the sliding dynamics of p53 in the slow mode. We propose that the loose and tight contacts of the core domains to DNA might be the origin of the multiple sliding modes of p53.

Discussion

In this investigation, we prepared the pseudo-WT p53 and examined the effect of the divalent cations on the 1D sliding dynamics along the stretched DNA. The effect of monovalent cations on the diffusion coefficient was examined previously for several DNA-binding proteins including p53 [5,32,33], and it was demonstrated that the potassium ion does not strongly affect the sliding dynamics of p53 [5]. In addition, early investigations demonstrated indirectly a possible role of Mg^{2+} in the sliding of the lac repressor [20,21]. However, there is no investigation so far to examine the effect of the divalent cations on the sliding process of p53. Since the concentration of the divalent cations changes significantly in cells that lost homeostatic control, the current investigation might provide new insight into the

physiological function of p53. We will discuss the implication of the current observations below.

We will first compare the data obtained in the ensemble experiments and the data obtained by the single-molecule measurements. The ensemble stopped-flow experiments showed that the apparent dissociation rate constant of pseudo-WT from 30-bp nspDNA is $74 \pm 4\ s^{-1}$ in the presence of 2 mM Mg^{2+} (Fig. 2b). The analysis of the dwell time of pseudo-WT on λDNA obtained in the single-molecule measurements based on the flow cell coated by the MPC polymer showed a major component dissociating with the dissociation rate constant of $19 \pm 1\ s^{-1}$ and a minor component dissociating rather slowly (Supplementary Fig. 11). The difference in the observations might be caused by the difference in the length of the DNAs used. It is also possible that the minor component identified in the single-molecule measurements might be missed in the stopped-flow experiments. We next calculated the fraction of the fast and slow modes in the single-molecule trajectories with various dwell times by fitting the displacement distributions of the pseudo-WT by Eq. (1). We confirmed that the fraction of the fast mode does not change (Supplementary Fig. 12). Accordingly, we suggest that the fast and slow sliding modes of p53 possess the similar dissociation rate constants.

The target search process of p53 under different concentrations of the divalent cations

We examined the equilibrium dissociation constant and the kinetic dissociation rate constant of the pseudo-WT p53 from the nonspecific sequence of DNA, and we observed that both equilibrium and kinetic properties of p53 depend on the concentration of the divalent cations. In particular, the apparent dissociation rate constant from the nspDNA increased for several times as we increase the concentration of Mg^{2+} and Ca^{2+} (Fig. 2b). In other words, the expected residence time of p53 on DNA should become shorter at the higher concentration of the divalent cations and might reduce the length of DNA that can be scanned by p53 in one binding event. We next clarified that the sliding dynamics of p53 becomes faster at the elevated concentration of the divalent cations (Fig. 4c). The faster sliding of p53 might accelerate the target search of p53. Thus, the divalent cations affect different steps of the target search process to the inverse directions.

To understand the overall effect of the divalent cations to the sliding dynamics of p53, we plotted the sliding distance of p53 on DNA, which is defined as the average size of DNA scanned per one binding event (see the supplementary text). Very impressively, the sliding distances of p53 estimated at various concentrations of the divalent cations are nearly constant and are within 140–250 bp, suggesting the shortened dissociation time at the elevated concentrations of the divalent cations is compensated for by the increased diffusion coefficient (Fig. 8). The sliding distances plotted should be considered as rough estimates and might underestimate the actual distances. To plot Fig. 8, we used the dissociation rate constants obtained in the ensemble experiment with the short DNA. As we discussed above, the ensemble rate constant obtained in the presence of 2 mM Mg^{2+} was several times faster than the rate constant estimated from the dwell time analysis of the single-molecule measurement under the corresponding condition (Supplementary Fig. 11). The difference might be attributable to the dissociation of p53 from the ends of the short DNA in the ensemble experiment. However, the plot in Fig. 8 suggests that the target search of p53 per one binding event is maintained under different concentrations of the divalent cations.

The efficient search for the binding sites of DNA-binding proteins including p53 is considered to be achieved by a combination of 1D sliding and three-dimensional (3D) search [5,34,35]. The 3D search enables p53 to alter the search region of DNA by transiently dissociating from DNA and then reassociating to the different regions of DNA. The 1D sliding enables p53 to move along DNA without dissociation as the 1D diffusion. In addition, the accuracy of the recognition of the target DNA also controls the search process. Further investigations are necessary to understand the effect of the divalent cations to the different steps in the target search process of p53. However, this investigation clearly demonstrated the effect of the divalent cations for the 1D sliding process of p53.

Mechanism of the accelerated diffusion of p53 in the presence of the divalent cations

Several possibilities can be proposed to explain the accelerated diffusion of p53 in the presence of

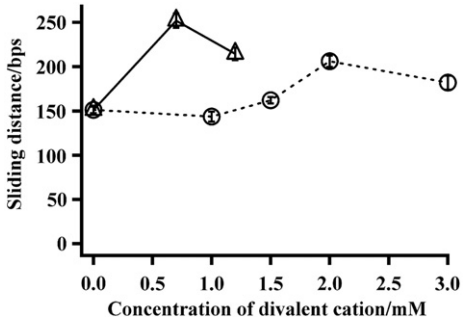


Fig. 8. The sliding distance expected for the pseudo-WT p53 after a single binding event to nspDNA. Triangles and circles represent data obtained in the presence of different concentrations of Ca^{2+} and Mg^{2+}, respectively.

the divalent cations. We note that there is no evidence supporting the specific binding of Mg^{2+} or Ca^{2+} to p53 except for the binding of Mg^{2+} to the open binding site of Zn^{2+} [36]. Under the experimental condition used in this study, however, Zn^{2+} should be tightly bound to p53, since an excess of ethylenediaminetetraacetic acid (EDTA) at more than 5 mM is required to remove Zn^{2+} from p53 [37]. Thus, we assume that the divalent cations act to DNA primarily, and we propose the following possible mechanisms in the order of likeliness.

First, the binding of the divalent cations to DNA might weaken the interaction between DNA and p53. Mg^{2+} and Ca^{2+} can bind specifically to phosphates and bases including guanine of DNA [14–19] and reduce the negative charges of the phosphate and may prevent the hydrogen bonds between the base and p53. Accordingly, the binding of the divalent cations to DNA might weaken the direct interaction between DNA and p53, resulting in the increase in the diffusion coefficient and the drift velocity of the fast mode, as well as the dissociation rate constant. It is also possible that the divalent cations bound to DNA might shift the conformation of p53 toward a faster sliding form, causing the fast sliding and dissociation. Second, the screening of the electrostatic interaction between DNA and p53 by the divalent cations might weaken the interaction and might accelerate the sliding [38]. However, the electrostatic screening of a monovalent cation does not affect the 1D sliding of p53 [5,6], suggesting that the electrostatic screening does not likely modulate the interaction between p53 and DNA. Third, a conformational change of DNA caused by the binding of the divalent cations or by the binding of p53 might modulate the sliding process. It is known that the B form of DNA is maintained at different concentrations of Mg^{2+} or Ca^{2+} in the range from zero to several millimolars, except for a minor bending of the bases caused by cation–π interactions [39,40]. However, it is still possible that a small conformational change of DNA such as bending caused by the binding of the divalent cations or p53 alters the sliding dynamics of p53. Thus, the binding of the divalent cations to DNA and the subsequent weakening of the DNA–p53 interaction are likely the origin of the accelerated diffusion of p53.

We propose that the multiple sliding modes of p53 are caused by the different interactions in the complex of p53 and DNA. The C-terminal domain of p53 promotes the sliding along DNA, while the core domain suppresses the sliding [5]. p53 has four core domains, which can contact with DNA nonspecifically [8]. We suggest that the sliding is promoted as the contact interaction decreases and that p53 possesses loose contacts of the core domains to DNA in the fast mode and tight contacts in the slow mode. To confirm the above suggestion, we constructed the coreless mutant and examined its sliding dynamics (Fig. 7 and see the supplementary text). The coreless mutant showed a single sliding mode having the diffusion coefficient larger than the fast mode of the pseudo-WT p53, supporting our suggestion that the different interactions between p53 and DNA involving the core domain are the origin of the two sliding modes.

The comparison of the diffusion coefficient for the two sliding modes of the pseudo-WT p53 and that for the coreless mutant suggests that the core domain may interact with DNA strongly in the slow mode and weakly in the fast mode. The multiple binding conformations of p53 in the p53–DNA complex have been suggested. For example, the electron microscopy studies demonstrate multiple quaternary structures of p53–DNA complex [41,42]. In addition, single-molecule Förster resonance energy transfer and NMR studies demonstrated that the core domain partly interacts with the C-terminal domain and the other core domains [43–45]. These interactions may regulate the conformational change of p53 on DNA. These results support our proposal that the loose and tight contacts of the core domains to DNA might be the origin of the multiple sliding modes of p53.

Tafvizi *et al*. suggested the presence of a hypothetical two modes, search and recognition modes, in the target search process of p53 [5]. It was discussed that the search and recognition modes exchange each other in the timescale of about 1 ms, which is much shorter than the transition time between the fast and slow modes identified in this investigation (more than 330 ms). Thus, we are in the opinion that the fast and slow modes do not correspond to the search and recognition modes proposed by Tafvizi *et al.* [5]. We suggest that the possible interactions between the core domains or between the core domain and the C-terminal domain in p53 might retard the transition between the two modes.

The multiple sliding modes were also observed in other DNA-binding proteins. A diverse diffusion coefficient in the 1D sliding was observed in LacI repressor, *E. coli* replisomes, and DNA glycosylases [46–48]. A paused motion was detected in bacterial UvrA/UvrB complexes and DNA glycosylases [49,50]. These proteins cover a wide range of oligomeric states from a monomer to more than tetramer. The data suggest that even monomeric proteins have a potential to possess loose and tight contacts to DNA, resulting in different sliding modes. Furthermore, the presence of multiple binding sites to DNA in one protein, such as dimeric or oligomeric proteins, might be one of the factors to cause multiple sliding modes. Thus, the presence of the multiple sliding modes might be a general observation for DNA-binding proteins including p53 and plays a pivotal role in their functions.

Physiological implications of the current observations

The concentrations of the divalent cations to alter the 1D sliding dynamics of p53 are in the range of the physiological concentrations. The total concentrations of Mg^{2+} and Ca^{2+} in nucleus/chromatin of a living cell were estimated to be 2–4 mM and 4–6 mM, respectively [51]. The total concentration of Mg^{2+} in mammalian cells ranges between 14 and 20 mM, and the concentration of free Mg^{2+} is 0.5–0.7 mM [52]. The concentration of free Ca^{2+} in the nucleus is 0.1–0.2 mM [53]. These results suggest that Mg^{2+} and Ca^{2+} could bind to DNA specifically in living cells, which might promote the movement of p53 along DNA.

The sliding dynamics of p53 might be regulated by the loss of homeostatic control for divalent cations. In apoptosis, the Ca^{2+} concentration is increased [11,12], which accelerates the sliding of p53 but reduces the binding time, and it eventually leads to a slight increase in the sliding distance of p53 (Fig. 8). In contrast, the Mg^{2+} deficiency in cell cycle arrest suppresses the sliding of p53 but increases the binding time, and it results in a small decrease of the sliding distance of p53 (Fig. 8). In both cases, the trade-off between the diffusion of the sliding and the binding time may not dramatically alter the search distance of p53 even in the loss of homeostatic control for divalent cations. However, the effect of divalent cations on the 3D search and/or the accuracy of the recognition should also regulate the efficiency and search time of p53 to the target sites. The current results demonstrating the effect of divalent cations to the 1D sliding call for the necessity of further investigations to understand the search mechanism of p53 relevant to physiological conditions.

Materials and Methods

Expression and purification of p53

The cDNA of human WT p53 and the artificially synthesized gene (Funakoshi, Co., Ltd.) for the thermostable and cysteine-modified mutant of human p53, the pseudo-WT (C124A, C135V, C141V, W146Y, C182S, V203A, R209P, C229Y, H233Y, Y234F, N235K, Y236F, T253V, N268D, C275A, C277A, K292C), were inserted into a plasmid, pGEX-6P-1. The WT and the pseudo-WT possess additional sequences GPLGSASKL and GPLGS at the N-terminus, respectively. These proteins were expressed in BL21(DE3)pLysS *E. coli* cells. The cells were cultured in 1 L of 2× YT media at 37 °C. After an OD_{600} of the culture reached 0.6, both IPTG and $ZnCl_2$ were added to the final concentration of 100 μM, and the cells were cultured at 20 °C for 20 h and harvested by centrifugation. The pellet was resuspended in the buffer containing 10 mM Na_2HPO_4, 1.8 mM KH_2PO_4, 2.7 mM KCl, 650 mM NaCl, 1 mM DTT, 10 mM $MgCl_2$, 1 mg/mL lysozyme, and 10 U/mL DNase (pH 7.4) and was lysed by sonication on ice. To remove DNA included in *E. coli*, we used 650 mM NaCl [54]. The lysed cells were further incubated on ice for 30 min. The supernatant was collected after centrifugation. GST-tagged p53 was purified by GST column (GSTrap™ FF; GE Healthcare, Tokyo, Japan). p53 was cleaved from the GST tag by Precission protease (GE Healthcare) in the column. The sample was further purified by heparin column (HiTrap™ Heparin HP; GE Healthcare). The expression and purification of p53 were confirmed by SDS-PAGE. Western blot analysis for the WT p53 was further conducted using two mouse monoclonal antibodies, p53(Pab240) and p53(DO-1) (Santa Cruz Biotechnology, Inc., Texas, USA). The elusion solution of p53 was stored at −80 °C.

Fluorescence anisotropy

Binding ability of p53 to DNA was quantitatively examined by using fluorescence anisotropy. Fluorometer (FP-6500; JASCO, Co., Tokyo, Japan) coupled with automatic titration accessory (ATS-443; JASCO, Co.) and home-built autorotating polarizer unit was used. p53 was titrated in the quartz cuvette including a fluorescence-labeled DNA at the concentration of 5 nM in the buffer containing 20 mM Hepes, 50 mM KCl, 2 mM $MgCl_2$, 0.5 mM EDTA, 1 mM DTT, and 0.5 mg BSA (pH 7.9) at 25 °C. The sequences of spDNA-FAM are 5′-6-FAM-ATCAGGAACATGTCCCAACATGTTGAGCTC-3′ and 3′-TAGTCCTTGTACAGGGTTGTACAACTCGAG-5′ (Sigma-Aldrich, Co., Tokyo, Japan). The underlined parts correspond to p21 promoter. The sequences of nspDNA-FAM are 5′-6-FAM-AATATGGTTTGAATAAAGAGTAAAGATTTG-3′ and 3′-TTATACCAAACTTATTTCTCATTTCTAAAC-5′ (Sigma-Aldrich, Co.), which was used for nonspecific binding. The excitation wavelength was 480 nm and the fluorescence of 525 nm was detected. A long-pass filter, which passes the wavelength longer than 500 nm, was used to prevent the scattered light from reaching the detector. All the measurements were finished within 50 min after the dilution of the stock solution to prevent the dissociation of the tetramer [27].

The observed data were analyzed by two-state binding model in which tetrameric p53 binds to DNA with a binding stoichiometry of 1:1. The observed anisotropy r_{obs} was fitted by using the equations:

$$r_{obs} = r_D \frac{(C_D - C_{pD})}{C_D} + r_{pD} \frac{C_{pD}}{C_D}, \quad (3)$$

$$C_{pD} = \frac{(C_D + C_p + K_D) - \sqrt{(C_D + C_p + K_D)^2 - 4C_D C_p}}{2}, \quad (4)$$

where r_D, r_{pD}, K_D, c_p, and c_D represent the anisotropy of free DNA, the anisotropy of p53–DNA complex, the apparent dissociation constant, the concentration of the tetrameric p53, and the concentration of DNA, respectively.

To measure the dissociation rate constant of p53 from nspDNA, we performed the stopped-flow kinetic fluorescence-anisotropy measurements by using a home-built system. An output from a 473-nm laser (Laser Quantum, Co., Ltd., Cheshire, UK) passed through a polarizer (Edmund Optics Japan, Co., Ltd., Tokyo, Japan) was introduced into the flow

cell of the stopped-flow apparatus (Unisoku, Co., Ltd., Osaka, Japan). The fluorescence from FAM was detected by a photosensor (H10722; Hamamatsu Photonics, KK, Hamamatsu, Japan) after passing through a polarizer (Edmund Optics Japan, Co., Ltd.) and a band-pass filter (FF01-520/35; Semrock, Inc., New York, USA). A mixture of p53 tetramer and nspDNA-FAM at concentrations 60 nM and 40 nM, respectively, was mixed with a solution of spDNA with no fluorescent dye at the concentration of 400 nM both in the buffer containing 20 mM Hepes, 50 mM KCl, 0–3 mM $MgCl_2$, 0.5 mM EDTA, 1 mM DTT, and 0.5 mg BSA at 25 °C and at pH 7.9. The mixing ratio was 1:1. The dead time was 1 ms. The dissociation of p53 from DNA was detected as decrease of the fluorescence anisotropy caused by the transfer of p53 from the fluorescent nspDNA to the nonfluorescent spDNA. Thus, two types of fluorescence intensity data, I_{VV} and I_{VH}, were detected at the same condition, where I_{VV} stands for the fluorescence intensity excited at the vertical polarization and detected at the vertical polarization, and I_{VH} stands for the fluorescence intensity excited at the vertical polarization and detected at the horizontal polarization. Several traces of $I_{VV}(t)$ and $I_{VH}(t)$ were independently measured as a function of time t. The time resolution was 1 ms. The time course of fluorescence anisotropy, $r(t)$, was calculated from the averaged traces of $I_{VV}(t)$ and $I_{VH}(t)$ based on Eq. (5):

$$r(t) = \frac{I_{VV}(t) - GI_{VH}(t)}{I_{VV}(t) + 2GI_{VH}(t)}. \quad (5)$$

I_{HV} represents the fluorescence intensity excited at the horizontal polarization and detected at the vertical polarization, and I_{HH} represents that excited at the horizontal polarization and detected at the horizontal polarization. The value of G factor, G, which was obtained from I_{HV} divided by I_{HH}, was 1. The trace of fluorescence anisotropy, $r(t)$, was then fitted with a single exponential, and the dissociation rate constant was obtained.

Labeling of fluorescent dye

The pseudo-WT p53 was labeled with ATTO532 (ATTO-TEC, GmbH, Siegen, Germany) using a maleimide chemistry. p53-ATTO532 was purified using cation-exchange column (HiTrap™ SP HP; GE Healthcare). The labeling ratio was determined as 1.4 dyes per a monomer of the mutant by observing the absorbances of 280 nm and 532 nm. The absorption coefficient of the p53 mutant is 30,350 M^{-1} cm^{-1} at 280 nm. p53-ATTO532 was stored at −80 °C.

Flow cell

The flow cell was constructed from a cover glass and a slide glass (Matsunami Glass Ind., Ltd., Osaka, Japan) [28]. The double-sided tape sealed the outer regions of the glasses to create the flow path between these glasses. Two holes were created in the slide glass using an electric drill before constructing the flow cell. One of the hole was connected to a syringe pump (μ-ton mini; Senshu Scientific, Co., Tokyo, Japan) through the PTFE tube whose inner diameter was 0.5 mm (GL Science, Tokyo, Japan), and the other hole was connected to a waste bottle. The connectors were purchased from Upchurch Scientific, Inc. (Oak Harbor, WA, USA). The flow cell was constructed from the slide glass and the coverslip was passivated with PEG-biotin and PEG [29,30]. We used 50 mg/mL of PEG-biotin (NANOCS, Inc., Massachusetts, USA) and 50 mg/mL of PEG for the coating to tether one end of λDNA on the coverslip.

Biotinylated λ duplex DNA

Biotin-11-dGTP (PerkinElmer, Inc., Massachusetts, USA) was introduced into both ends of λDNA (NEW ENGLAND BioLabs, Inc., Massachusetts, USA) by the end-filling reaction with Klenow exo− (NEW ENGLAND BioLabs, Inc.).

TIRF microscopy

An output of a 532-nm laser (CL532-050-L; CrystaLaser, Nevada, USA) was 10 times expanded and collimated on the back focal plane of an objective lens with *N.A.* at 1.4 (Nikon, Tokyo, Japan) using a spherical lens (f = 500 mm). The flow cell was placed in front of the objective lens. The excitation light was introduced through the peripheral portion of the objective lens corresponding to *N.A.* at around 1.40. The alignment enables to illuminate the sample with the total internal reflection mode. The fluorescence was collected by the same objective and was imaged by TDI-EM CCD camera (Hamamatsu Photonics, KK, Hamamatsu, Japan) after passing through the dichroic mirror and a spatial filter unit. The dichroic mirror (Di01-R405/488/532/635-25×36; Semrock, Inc.) was placed between the objective lens and the spherical lens so as to split the excitation light and the fluorescence from p53 on DNA. The spatial filter unit (Optonica, Co., Kyoto, Japan) is composed of a slit and two multiple lenses (f = 200 and 70 mm). An optical filter (BLP01-532R-24; Semrock, Inc.) was mounted between the spatial filter unit and the camera. A spherical lens (f = 70 mm) was used to focus the fluorescence on the camera. The final magnification of the image was 100×. The laser power was 0.2 mW.

Single-molecule measurements

A neutravidin solution at 0.2 mg/mL in a buffer containing 25 mM Tris–HCl and 50 mM NaCl at pH 7.5 was introduced into the PEG-biotin-coated flow cell and incubated for 30 min to construct the neutravidin-coated flow cell [6,29,30]. To prevent nonspecific binding of p53 to the surface, we introduced the blocking buffer containing 20 mM Tris–HCl, 50 mM NaCl, 2 mM EDTA, and 10 mg/mL BSA at pH 7.5 and incubated it for 30 min. The biotinylated λDNA in the buffer containing 20 mM Tris–HCl, 50 mM NaCl, 2 mM EDTA, and 1 mg/mL BSA at pH 7.5 was then introduced into the neutravidin-coated flow cell at a concentration of 30 pM and incubated for 20–30 min to tether one end of DNA on the coverslip. Untethered DNA was then washed out by introducing the same solution. The number of the tethered DNAs was 5–20 in the field of view with a diameter of 30 μm. The pseudo-WT p53 in the buffer containing 20 mM Hepes, 0.5 mM EDTA, and 0–3 mM $MgCl_2$ or 0–1.5 mM $CaCl_2$, 0.5 mM DTT, 2 mM trolox, and 0.5 mg/mL BSA at pH 7.9 was introduced at the concentration of 0.5–2 nM at the rate of 500 μL/min, and the single-molecule measurements were performed. The dilution of p53 from the stock solution at 10 μM to the abovementioned solution at

0.5–2 nM was performed immediately before the experiments. All the measurements were finished within 50 min after the dilution of the stock solution to prevent the dissociation of the tetramer [27]. The concentrations of free Mg^{2+} and Ca^{2+} in the solution were estimated using a concentration-sensitive fluorescent dye, mag-fura-2. The inaccuracies of Mg^{2+} concentrations in our experiments were within 0.2 mM.

Analysis of single-molecule data

A software ImageJ and its plugin, particle track and analysis, were used to track the center of the fluorescent spots based on two-dimensional Gaussian fitting. The two-dimensional trajectories were rotated to adjust the longitudinal and traverse axes of the DNA to the *x*-axis and *y*-axis, respectively. The positions of p53 were represented by x_i and y_i with the data point *i*. Firstly, the trajectories with more than 15 data points were selected. Secondly, we chose the trajectories that satisfy the following criteria to exclude the trajectories of p53 adsorbed on the coverslip. The local MSD of every segments with 10 data points in the trajectories $\langle(x_{i+5} - x_i)^2\rangle$ was calculated and the trajectories in which all the values of the local MSDs are larger than 0.0015 μm^2. This threshold corresponds to 84% in cumulative distribution of the local MSDs in the absorbed molecules. Thirdly, we removed the trajectories whose $|x_{i+1} - x_i|$ is larger than 300 nm because these are likely due to misconnection between the trajectory of a molecule and that of the other molecule.

Acknowledgements

A. Murata, S. Takahashi, and K. Kamagata thank Prof. Akihiko Ishijima, Dr. Yuichi Inoue, Dr. Hajime Fukuoka, Dr. Kumiko Hayashi, Dr. Hiroyuki Oikawa (Tohoku University), Prof. Chun Biu, Lee (Hokkaido University), Prof. Junichiro Futami (Okayama University), Prof. Hidehiro Oana (University of Tokyo), Prof. Nobuo Shimamoto (Kyoto-Sangyo University), Prof. Shoji Takada, and Dr. Tsuyoshi Terakawa (Kyoto University) for helpful discussions; Prof. Fumi Nagatsugi (Tohoku University) for electrophoretic mobility shift assay; and Dr. Eriko Mano (Tohoku University) for expression of p53. This work was supported by Japan Science and Technology Agency/CREST and Grants-in-Aid for Scientific Research from the Ministry of Education, Culture, Sports, Science, and Technology of Japan (to K. Kamagata and S. Takahashi) and Grant for Basic Science Research Projects from The Sumitomo Foundation (to K. Kamagata).

Appendix A. Supplementary data

Supplementary data to this article can be found online at http://dx.doi.org/10.1016/j.jmb.2015.06.016.

Received 4 February 2015;
Received in revised form 27 May 2015;
Accepted 25 June 2015
Available online 2 July 2015

Keywords:
p53;
single-molecule;
DNA;
sliding;
divalent cation

Present address: R. Kashima, Cardiovascular Research Institute, University of California, San Francisco, CA 94158, USA.

Present address: K. Nanatani, Department of Microbial Resources, Graduate School of Agricultural Science, Tohoku University, Sendai 981-8555, Japan.

Abbreviations used:
1D, one-dimensional; TIRF, total internal reflection fluorescence; MPC, 2-methacryloyloxyethyl phosphorylcholine; MSD, mean square displacement; PEG, polyethylene glycol; 3D, three-dimensional; EDTA, ethylenediaminetetraacetic acid.

References

[1] B. Vogelstein, D. Lane, A.J. Levine, Surfing the p53 network, Nature 408 (2000) 307–310.
[2] C.J. Brown, S. Lain, C.S. Verma, A.R. Fersht, D.P. Lane, Awakening guardian angels: drugging the p53 pathway, Nat. Rev. Cancer 9 (2009) 862–873.
[3] A.C. Joerger, A.R. Fersht, The tumor suppressor p53: from structures to drug discovery, Cold Spring Harb. Perspect. Biol. 2 (2010) a000919.
[4] Y. Jiao, D.I. Cherny, G. Heim, T.M. Jovin, T.E. Schäffer, Dynamic interactions of p53 with DNA in solution by time-lapse atomic force microscopy, J. Mol. Biol. 314 (2001) 233–243.
[5] A. Tafvizi, F. Huang, A.R. Fersht, L.A. Mirny, A.M. van Oijen, A single-molecule characterization of p53 search on DNA, Proc. Natl. Acad. Sci. U. S. A. 108 (2011) 563–568.
[6] A. Tafvizi, F. Huang, J.S. Leith, A.R. Fersht, L.A. Mirny, A.M. van Oijen, Tumor suppressor p53 slides on DNA with low friction and high stability, Biophys. J. 95 (2008) L01–L03.
[7] J.S. Leith, A. Tafvizi, F. Huang, W.E. Uspal, P.S. Doyle, A.R. Fersht, L.A. Mirny, A.M. van Oijen, Sequence-dependent sliding kinetics of p53, Proc. Natl. Acad. Sci. U. S. A. 109 (2012) 16552–16557.
[8] T. Terakawa, H. Kenzaki, S. Takada, p53 searches on DNA by rotation-uncoupled sliding at C-terminal tails and restricted hopping of core domains, J. Am. Chem. Soc. 134 (2012) 14555–14562.
[9] P. Nicotera, B. Zhivotovsky, S. Orrenius, Nuclear calcium transport and the role of calcium in apoptosis, Cell Calcium 16 (1994) 279–288.
[10] M.J. Berridge, M.D. Bootman, P. Lipp, Calcium—a life and death signal, Nature 395 (1998) 645–648.
[11] Q.L. Zhao, T. Kondo, A. Noda, Y. Fujiwara, Mitochondrial and intracellular free-calcium regulation of radiation-induced

apoptosis in human leukemic cells, Int. J. Radiat. Biol. 75 (1999) 493–504.
[12] R. Gogna, E. Madan, B. Keppler, U. Pati, Gallium compound GaQ(3)-induced Ca(2+) signalling triggers p53-dependent and -independent apoptosis in cancer cells, Br. J. Pharmacol. 166 (2012) 617–636.
[13] A. Ikari, H. Sawada, A. Sanada, C. Tonegawa, Y. Yamazaki, J. Sugatani, Magnesium deficiency suppresses cell cycle progression mediated by increase in transcriptional activity of p21(Cip1) and p27(Kip1) in renal epithelial NRK-52E cells, J. Cell. Biochem. 112 (2011) 3563–3572.
[14] A.Z. Li, H. Huang, X. Re, L.J. Qi, K.A. Marx, A gel electrophoresis study of the competitive effects of monovalent counterion on the extent of divalent counterions binding to DNA, Biophys. J. 74 (1998) 964–973.
[15] V. Tereshko, G. Minasov, M. Egli, The Dickerson-Drew B-DNA dodecamer revisited at atomic resolution, J. Am. Chem. Soc. 121 (1999) 470–471.
[16] G. Minasov, V. Tereshko, M. Egli, Atomic-resolution crystal structures of B-DNA reveal specific influences of divalent metal ions on conformation and packing, J. Mol. Biol. 291 (1999) 83–99.
[17] T.K. Chiu, R.E. Dickerson, 1 Å crystal structures of B-DNA reveal sequence-specific binding and groove-specific bending of DNA by magnesium and calcium, J. Mol. Biol. 301 (2000) 915–945.
[18] N.V. Hud, M. Polak, DNA–cation interactions: the major and minor grooves are flexible ionophores, Curr. Opin. Struct. Biol. 11 (2001) 293–301.
[19] R. Ahmad, H. Arakawa, H.A. Tajmir-Riahi, A comparative study of DNA complexation with Mg(II) and Ca(II) in aqueous solution: major and minor grooves bindings, Biophys. J. 84 (2003) 2460–2466.
[20] O.G. Berg, C. Blomberg, Association kinetics with coupled diffusion III. Ionic-strength dependence of the lac repressor-operator association, Biophys. Chem. 8 (1978) 271–280.
[21] M.D. Barkley, Salt dependence of the kinetics of the lac repressor–operator interaction: role of nonoperator deoxyribonucleic acid in the association reaction, Biochemistry 20 (1981) 3833–3842.
[22] A.N. Bullock, J. Henckel, B.S. DeDecker, C.M. Johnson, P.V. Nikolova, M.R. Proctor, D.P. Lane, A.R. Fersht, Thermodynamic stability of wild-type and mutant p53 core domain, Proc. Natl. Acad. Sci. U. S. A. 94 (1997) 14338–14342.
[23] T.J. Petty, S. Emamzadah, L. Costantino, I. Petkova, E.S. Stavridi, J.G. Saven, E. Vauthey, T.D. Halazonetis, An induced fit mechanism regulates p53 DNA binding kinetics to confer sequence specificity, EMBO J. 30 (2011) 2167–2176.
[24] S. Bell, S. Hansen, J. Buchner, Refolding and structural characterization of the human p53 tumor suppressor protein, Biophys. Chem. 96 (2002) 243–257.
[25] M.E. Anderson, B. Woelker, M. Reed, P. Wang, P. Tegtmeyer, Reciprocal interference between the sequence-specific core and nonspecific C-terminal DNA binding domains of p53: implications for regulation, Mol. Cell. Biol. 17 (1997) 6255–6264.
[26] R.L. Weinberg, S.M. Freund, D.B. Veprintsev, M. Bycroft, A.R. Fersht, Regulation of DNA binding of p53 by its C-terminal domain, J. Mol. Biol. 342 (2004) 801–811.
[27] S. Rajagopalan, F. Huang, A.R. Fersht, Single-molecule characterization of oligomerization kinetics and equilibria of the tumor suppressor p53, Nucleic Acids Res. 39 (2011) 2294–2303.
[28] A.M. van Oijen, P.C. Blainey, D.J. Crampton, C.C. Richardson, T. Ellenberger, X.S. Xie, Single-molecule kinetics of lambda exonuclease reveal base dependence and dynamic disorder, Science 301 (2003) 1235–1238.
[29] J.B. Lee, R.K. Hite, S.M. Hamdan, X.S. Xie, C.C. Richardson, A.M. van Oijen, DNA primase acts as a molecular brake in DNA replication, Nature 439 (2006) 621–624.
[30] A.L. Forget, S.C. Kowalczykowski, Single-molecule imaging of DNA pairing by RecA reveals a three-dimensional homology search, Nature 482 (2012) 423–427.
[31] P.S. Doyle, B. Ladoux, J.L. Viovy, Dynamics of a tethered polymer in shear flow, Phys. Rev. Lett. 84 (2000) 4769–4772.
[32] P.C. Blainey, A.M. van Oijen, A. Banerjee, G.L. Verdine, X.S. Xie, A base-excision DNA-repair protein finds intrahelical lesion bases by fast sliding in contact with DNA, Proc. Natl. Acad. Sci. U. S. A. 103 (2006) 5752–5757.
[33] G. Komazin-Meredith, R. Mirchev, D.E. Golan, A.M. van Oijen, D.M. Coen, Hopping of a processivity factor on DNA revealed by single-molecule assays of diffusion, Proc. Natl. Acad. Sci. U. S. A. 105 (2008) 10721–10726.
[34] S.E. Halford, J.F. Marko, How do site-specific DNA-binding proteins find their targets? Nucleic Acids Res. 32 (2004) 3040–3052.
[35] M. Slutsky, L.A. Mirny, Kinetics of protein–DNA interaction: facilitated target location in sequence-dependent potential, Biophys. J. 87 (2004) 4021–4035.
[36] Y. Xue, S. Wang, X. Feng, Influence of magnesium ion on the binding of p53 DNA-binding domain to DNA-response elements, J. Biochem. 146 (2009) 77–85.
[37] E. Paleček, V. Ostatná, H. Černocká, A.C. Joerger, A.R. Fersht, Electrocatalytic monitoring of metal binding and mutation-induced conformational changes in p53 at picomole level, J. Am. Chem. Soc. 133 (2011) 7190–7196.
[38] T.M. Lohman, Kinetics of protein–nucleic acid interactions: use of salt effects to probe mechanisms of interaction, CRC Crit. Rev. Biochem. 19 (1986) 191–245.
[39] J. Duguid, V.A. Bloomfield, J. Benevides, G.J. Thomas, Raman spectroscopy of DNA–metal complexes. I. Interactions and conformational effects of the divalent cations: Mg, Ca, Sr, Ba, Mn, Co, Ni, Cu, Pd, and Cd, Biophys. J. 65 (1993) 1916–1928.
[40] L. McFail-Isom, X. Shui, L.D. Williams, Divalent cations stabilize unstacked conformations of DNA and RNA by interacting with base pi systems, Biochemistry 37 (1998) 17105–17111.
[41] R. Melero, S. Rajagopalan, M. Lázaro, A.C. Joerger, T. Brandt, D.B. Veprintsev, G. Lasso, D. Gil, S.H. Scheres, J.M. Carazo, A.R. Fersht, M. Valle, Electron microscopy studies on the quaternary structure of p53 reveal different binding modes for p53 tetramers in complex with DNA, Proc. Natl. Acad. Sci. U. S. A. 108 (2011) 557–562.
[42] R. Aramayo, M.B. Sherman, K. Brownless, R. Lurz, A.L. Okorokov, E.V. Orlova, Quaternary structure of the specific p53–DNA complex reveals the mechanism of p53 mutant dominance, Nucleic Acids Res. 39 (2011) 8960–8971.
[43] D.B. Veprintsev, S.M. Freund, A. Andreeva, S.E. Rutledge, H. Tidow, J.M. Cañadillas, C.M. Blair, A.R. Fersht, Core domain interactions in full-length p53 in solution, Proc. Natl. Acad. Sci. U. S. A. 103 (2006) 2115–2119.
[44] F. Huang, S. Rajagopalan, G. Settanni, R.J. Marsh, D.A. Armoogum, N. Nicolaou, A.J. Bain, E. Lerner, E. Haas, L. Ying, A.R. Fersht, Multiple conformations of full-length p53 detected with single-molecule fluorescence resonance energy transfer, Proc. Natl. Acad. Sci. U. S. A. 106 (2009) 20758–20763.

[45] M. Bista, S.M. Freund, A.R. Fersht, Domain–domain interactions in full-length p53 and a specific DNA complex probed by methyl NMR spectroscopy, Proc. Natl. Acad. Sci. U. S. A. 109 (2012) 15752–15756.
[46] Y.M. Wang, R.H. Austin, E.C. Cox, Single molecule measurements of repressor protein 1D diffusion on DNA, Phys. Rev. Lett. 97 (2006) 048302.
[47] N.Y. Yao, R.E. Georgescu, J. Finkelstein, M.E. O'Donnell, Single-molecule analysis reveals that the lagging strand increases replisome processivity but slows replication fork progression, Proc. Natl. Acad. Sci. U. S. A. 106 (2009) 13236–13241.
[48] A.R. Dunn, N.M. Kad, S.R. Nelson, D.M. Warshaw, S.S. Wallace, Single Qdot-labeled glycosylase molecules use a wedge amino acid to probe for lesions while scanning along DNA, Nucleic Acids Res. 9 (2011) 7487–7498.
[49] N.M. Kad, H. Wang, G.G. Kennedy, D.M. Warshaw, B.V. Houten, D.N.A. Collaborative Dynamic, Scanning by nucleotide excision repair proteins investigated by single-molecule imaging of quantum-dot-labeled proteins, Mol. Cell 37 (2010) 702–713.
[50] S.R. Nelson, A.R. Dunn, S.D. Kathe, D.M. Warshaw, S.S. Wallace, Two glycosylase families diffusively scan DNA using a wedge residue to probe for and identify oxidatively damaged bases, Proc. Natl. Acad. Sci. U. S. A. 111 (2014) E2091–E2099.
[51] R. Strick, P.L. Strissel, K. Gavrilov, R. Levi-Setti, Cation–chromatin binding as shown by ion microscopy is essential for the structural integrity of chromosomes, J. Cell Biol. 155 (2001) 899–910.
[52] A. Romani, Regulation of magnesium homeostasis and transport in mammalian cells, Arch. Biochem. Biophys. 458 (2007) 90–102.
[53] B. Himpens, H. De Smedt, R. Casteels, Relationship between [Ca^{2+}] changes in nucleus and cytosol, Cell Calcium 16 (1994) 239–246.
[54] A.I. Coffer, P.P. Knowles, Divalent metal ions induce conformational change in pure, human wild-type p53 tumor suppressor protein, Biochim. Biophys. Acta 1209 (1994) 279–285.